Journal of
Synchrotron Radiation

ISSN 0909-0495

Received 9 October 2008
Accepted 21 May 2009

A soft X-ray beamline for transmission X-ray microscopy at ALBA

E. Pereiro,* J. Nicolás, S. Ferrer and M. R. Howells

ALBA Light Source, Carretera de Cerdanyola del Vallès a Sant Cugat, BP 1413, Km 3.3, 08290 Cerdanyola del Vallès, Barcelona, Spain. E-mail: epereiro@cells.es

The MISTRAL beamline is one of the seven phase-I beamlines at the ALBA synchrotron light source (Barcelona, Spain) that will be opened to users at the end of 2010. MISTRAL will be devoted to cryotomography in the water window and multi-keV spectral regions for biological applications. The optics design consists of a plane-grating monochromator that has been implemented using variable-line-spacing gratings to fulfil the requirements of X-ray microscopy using a reflective condenser. For instance, a fixed-focus condition independent of the included angle, constant magnification as well as coma and spherical aberration corrections are achieved with this system. The reported design is of wider use.

Keywords: X-ray microscopy; tomography; Kirkpatrick–Baez mirrors; variable-line-spacing gratings; plane-grating monochromator.

1. Introduction

X-ray microscopes, both imaging and scanning, have been in use on synchrotrons for more than three decades. During that time the beamlines used to illuminate the microscope sample have tended to follow established designs. For the case of the imaging microscope or transmission X-ray microscope (TXM), which is the case of interest to us, this has usually involved a bending-magnet source, a power-filtering plane mirror and a condenser zone plate. The latter, in combination with a pinhole, functions as a moderate-resolution monochromator (Niemann *et al.*, 1974) and also delivers a focused X-ray beam onto the sample with the intention of providing a 'critical illumination' (Born & Wolf, 1980). Beamlines of this type are not easily or rapidly wavelength-tunable and have tended to operate at a constant water window wavelength (see below) for long periods of time.

In the recent past, and especially since the Eighth International Conference on X-ray Microscopy at Himeji in 2005, several new trends have become evident which are bringing major changes to TXMs and the beamlines that are needed to feed them.

(i) TXMs have always had the advantage of multiplexed data collection, but this is now beginning to be seriously exploited for tomographic studies.

(ii) Such tomographic studies have great potential for biological imaging provided that samples can be damage-protected by imaging at cryogenic temperatures (Schneider *et al.*, 2002).

(iii) The so-called 'mono-capillary' reflective condenser (Zheng *et al.*, 2008) has been demonstrated at several beamlines (Tang *et al.*, 2006; Yin *et al.*, 2006; Schneider *et al.*, 2006; Andrews *et al.*, 2008), and promises to make TXMs easier to build and much more wavelength-tunable. However, its durability, high efficiency, capability to match the numerical aperture of all current objective zone plates and other advantages must be bought at the price of providing a separate monochromator.

(iv) TXMs are being operated at multi-keV X-ray energies and broader energy ranges, requiring beamlines that can deliver tunable monochromatic X-rays over such ranges.

The ALBA X-ray microscopy program is driven by the needs of a biological community for a new-style TXM with capability for cryotomography in the water window and multi-keV spectral regions. This will require several capillary condensers and a completely new approach to designing an X-ray microscopy beamline. In the following we report our proposed solution to this design problem. It has been developed in the context of the ALBA synchrotron facility but is of wider application.

2. X-ray microscopy at ALBA

The ALBA synchrotron radiation facility will be opened for users at the end of 2010. It is a 3 GeV low-emittance storage ring able to run in top-up mode. The storage ring is planned to be operated at a nominal current of 250 mA, although in the future it is foreseen to operate at a maximum of 400 mA. One of the beamlines in the first construction phase is the X-ray microscopy beamline (MISTRAL), which will be dedicated to full-field imaging of frozen-hydrated biological samples from 270 eV to 2600 eV.

X-ray microscopy (XRM) has been shown to provide insight into the internal structure of whole cells (Schneider,

1998; Larabell & Le Gros, 2004). The aim of XRM in combination with other techniques is to be able to locate subcellular structures at the time of key cellular events. For this purpose, the water window spectral range, between the inner-shell absorption edges of carbon (284 eV) and oxygen (543 eV), is one approach for imaging biological samples because water layers of thickness 10–15 μm can be penetrated while organic cell structures can be visualized with good absorption contrast. Specimens can thus be imaged in the hydrated state without modification except for vitrification of the water *via* a cryo-fixation process. Moreover, even thicker samples can be imaged by means of phase contrast at multi-keV energies. Increasing the working energy also provides other advantages. It increases the depth of focus (DoF), which is a limiting parameter in high-resolution microscopy. Having a DoF greater than the sample size avoids a form of resolution blurring that currently limits the resolution in X-ray tomography at lower energies such as the water window. Higher-energy X-rays also extend the focal length of the objective lens which greatly simplifies the sample rotation needed for tomography.

In addition to tomography, it is also interesting to perform spectroscopic imaging (a series of two-dimensional images over a range of X-ray wavelengths) at several interesting X-ray absorption edges (*i.e.* C, N, O, Ca, Fe, Cu, Mg, P, S). While full-field imaging in absorption or phase contrast requires monochromatic illumination of the sample with moderate resolution (based on the number of zone-plate zones; Thieme, 1988), a somewhat smaller bandwidth is required for spectroscopy (determined by the energy spread of NEXAFS spectral features; Zhang *et al.*, 2003).

3. Functional description of the beamline

The MISTRAL beamline and monochromator are designed to provide uniform energy-independent illumination to the reflective condenser optics, and high flux in the range between 270 eV and 2600 eV using a bending-magnet (BM) source. This imposes several conditions as follows.

(i) There must be a stigmatic image of the source at the (fixed) exit slit plane, for all X-ray energies.

(ii) The beam emerging from the exit slit must provide uniform illumination of the entrance aperture of the reflective capillary condenser and, to the extent possible, must match the shape of the aperture.

(iii) The solid angle from the source accepted by the beamline optics must be approximately 1.2 mrad × 1.2 mrad to provide sufficient photon flux.

The fixed-focus condition and constant magnification can be achieved with a collimated light SX700 system (Follath & Senf, 1997). However, the vertical width of the beam from an ALBA BM arriving into the experimental floor is more than 1 cm high, much too large for practical SX700 systems. A solution to this is to focus the beam vertically onto an entrance slit and then locate the grating a fairly short distance downstream of that slit. This would still allow the use of the standard SX700 plane-grating monochromator (Petersen, 1982), which can provide fixed vertical demagnification and fixed-focus position if the included angle is chosen to keep the fixed-focus factor c_{ff} constant (where c_{ff} is the ratio of the cosine of the diffracted angle β to the cosine of the incident angle α where α and β are measured from the normal; see Appendix *A* for more details). In the case of MISTRAL, however, a significant improvement with respect to the original SX700 monochromator is introduced: it uses variable-line-spacing gratings (VLS) designed to keep the exit slit in focus for any value of the included angle, as well as to correct the coma and spherical aberration of the system. This preserves the stigmatic focus at the exit slit even for different values of c_{ff}, and provides flexibility for trading off spectral resolution with flux or harmonic rejection. Having thus established the basic architecture of the beamline, we now turn to fixing the design parameters.

3.1. Choice of beamline parameters

Polychromatic radiation will be delivered by a BM with field strength of 1.42 T, critical energy of 8.5 keV and critical wavelength of 0.15 nm. The BM will provide a source size of 133.3 μm and 76.4 μm FWHM horizontally (H) and vertically (V), respectively.

The variable-line-spacing plane-grating monochromator (VLS PGM) discussed above will deliver monochromatic light to the reflective capillary condenser, which will focus the light onto the sample. The transmitted X-ray beam will be collected by an objective Fresnel zone plate and a magnified image will be delivered to a CCD.

It is desired that the X-ray beam illuminates a relatively large field of view (*e.g.* $\geq$10 μm) and that its angular divergence should be large enough to fill the angular acceptance of the objective zone plate. In fact, a synchrotron source generally provides an emittance (defined as the product of the beam divergence and the beam size) which is smaller than the phase-space acceptance of the microscope (phase-space mismatch). This phase-space mismatch is much greater (worse) with undulators than with BMs. The common practice is to choose the angle to match the numerical aperture (NA) of the objective zone plate and wobble the incoming beam, by raster-scanning the condenser lens, to fill the sample with light. The period of the raster scan must therefore be a few times shorter than the exposure time. Currently the condenser scanner is a pair of *X* and *Y* piezo-driven flexures operating at a few tens of Hz.

A fan of radiation of 1.2 mrad (H) × 1.2 mrad (V) will be used to supply X-ray energies in the range 270–2600 eV. The vertical angle is chosen to collect the vertical FWHM at the lowest energies, while at the highest energies the required collection angle diminishes to approximately 0.5 mrad. The collected fan from the BM will pass through the beamline front end and the shield wall into an optics hutch containing two mirrors in Kirkpatrick–Baez (KB) geometry (KB system). The first mirror, VFM (vertical focusing mirror), of this KB pair will reflect in the vertical plane and will focus light from the source onto the monochromator entrance slit S_{in} (see Fig. 1). The second mirror, HFM (horizontal focusing mirror),

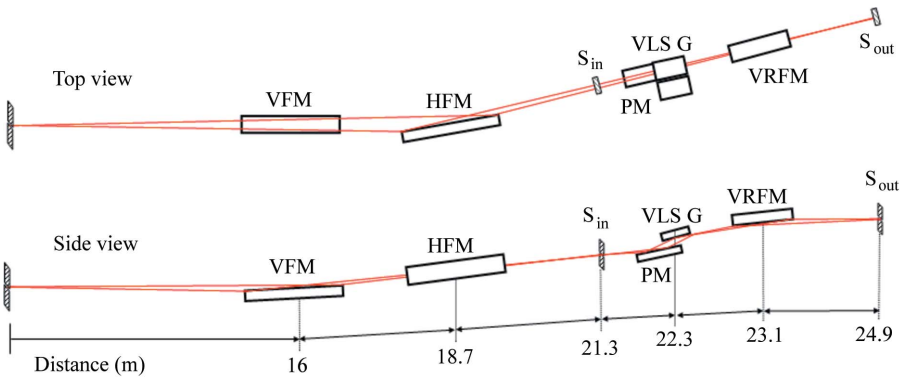

Figure 1
Beamline layout showing the KB pair, where VFM focuses vertically onto the entrance slit (S_{in}) and HFM horizontally onto the exit slit (S_{out}), the vertically dispersing VLS PGM constituted by a plane mirror PM, two VLS plane gratings G (only shown in the top view) and an elliptical refocusing mirror VRFM. The PGM can work at constant magnification while S_{in} and S_{out} are kept fixed. The deflection angle is 2.4° for VFM, HFM and VRFM.

will reflect in the horizontal plane and will focus light from the source onto the monochromator exit slit S_{out} (see Fig. 1). Both VFM and HFM have been chosen to have a magnification equal to 1/3.

A vertically dispersive VLS PGM, comprising a plane mirror PM, two VLS gratings, an elliptical cylinder refocusing mirror VRFM (vertical refocusing mirror) and entrance and exit slits, will provide monochromatic light to the capillary condenser (see Fig. 1). A constant slit-to-slit magnification in the dispersion plane of $1/c_{ff}$ with c_{ff} = 2.25 (for standard operation) will be used in positive diffraction order. Imaging requires only a moderate resolving power of 500–1000 which corresponds to the typical number of zones of an objective Fresnel zone plate (Thieme, 1988). For standard imaging operation, the vertically defining exit slit (S_{out}) will have an opening of 15 µm; the entrance slit (S_{in}) will be set at 30 µm which fits the threefold-demagnified FWHM vertical source size. Fig. 1 shows the beamline optical layout up to the experimental hutch. From this diagram we also define the object and image distances for the grating: $r = -r' = \mathrm{G} - \mathrm{S_{in}}$.

4. VLS PGM

4.1. General description of the VLS PGM

We have chosen to have an entrance slit at 1.0 m from the grating. This is sufficient to achieve the moderate resolution that we require and produces a vertical beam size arriving at the grating that is generally not more than 3 mm, which is within the capability of standard commercial realisations of PGMs. Our system is a VLS version of the original SX700 (Petersen, 1982) with an entrance slit. It has some optical advantages compared with the original one but is mechanically identical.

Fig. 2 shows the PGM scheme constituted by a plane mirror PM and a VLS plane grating G. The energy scan is performed by rotation of PM and G around their rotation axes R_{PM} and R_G, respectively (see Fig. 2). The rotation axis of the grating is at its center, while the rotation axis of the PM is chosen so that the incoming principal ray is made to pass through the grating axis R_G with better than 10 µm accuracy, by setting $Z_{PM} = 1.5Z_G$, $Y_{PM} \simeq 0$. The offset $h = Z_G$ between the incoming and outgoing beam is 15 mm.

4.2. VLS gratings

The monochromator must cover continuously the range of energies between 270 eV and 2600 eV. We define the groove spacing of the VLS grating for a general point $P(w, l)$ (see Fig. 3) as

$$d(w) = d_0\left(1 + \nu_1 w + \nu_2 w^2 + \ldots\right).$$

More information on the VLS monochromator and grating design is provided in Appendix *A*. The parameters are indicated in Table 1.

The VLS coefficients were determined by the theory described in Appendix *A* while the groove shapes (last two columns of Table 1) were optimized for efficiency using the Nevière method as implemented in the BESSY computer code *REFLEC* (Schäfers & Krumrey, 1996). Two VLS gratings will

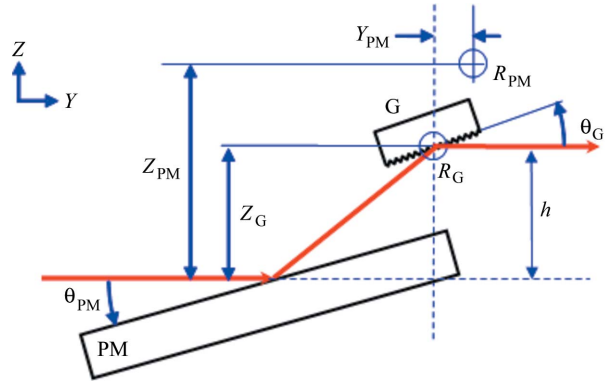

Figure 2
Scheme of the plane-grating monochromator.

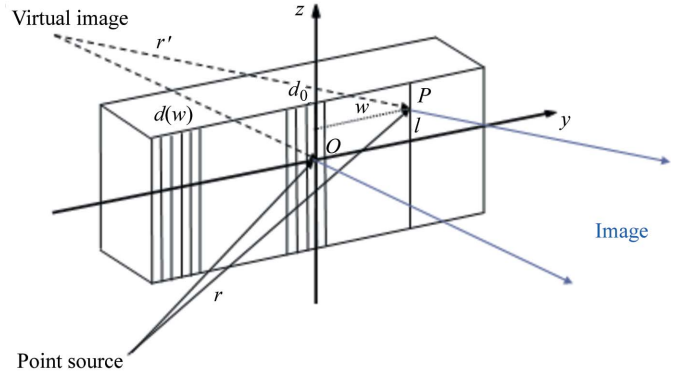

Figure 3
Schematic view of the variable-line-spacing grating. The typical point on the surface is $P(w, l)$.

Table 1
Grating profile parameters for the two energy ranges.

G	Minimum E (eV)	Maximum E (eV)	Groove density (both gratings)	Groove depth	Groove-to-period ratio
G1 (Rh)	800	2600	$d_0 = 0.000167$ cm	65 Å	0.5
G2 (Ni)	270	800	$\nu_1 = -0.02$ cm^{-1}	120 Å	0.5
			$\nu_2 = 0.0001$ cm^{-2}		
			$\nu_3 = 0$ cm^{-3}		
			$\nu_4 = 0$ cm^{-4}		

cover the desired energy range and will have Ni and Rh coatings for the low-energy range (LE: 270–800 eV) and the high energy range (HE: 800–2600 eV), respectively.

Finally, for tangential focusing of the virtual image onto the exit slit an elliptical cylinder mirror VRFM (see Fig. 1) is used in approximately 1:1 geometry.

5. Discussion

Tomography is a flux-intensive technique. The expected flux at the sample position has been estimated, taking into account the wobbling of the capillary needed to fill the sample (*i.e.* 10 µm × 10 µm) with light and the efficiencies of the optical components (see Fig. 4). All the mirrors have two coating stripes of Ni and Rh for the LE and HE range, respectively.

The radiation dose needed for a two-dimensional image of a 20 nm cube of protein in various ice thicknesses as a function of X-ray energy is shown in Fig. 5. The calculation is by C. Jacobsen (Howells *et al.*, 2007), following previous similar calculations by Kirz *et al.* (1995), and the optical quality is taken to satisfy the Rose criterion (Rose, 1948) (*i.e.* signal-to-noise ratio = 5 or 25 X-rays per voxel). Let us consider the effect of using a dose of 10^8 Gy. From Fig. 5, this is about twice that needed for Rose-criterion image quality at 20 nm resolution over much of the energy range. However, the resolution goal for routine use of the MISTRAL beamline is 30 nm and not 20 nm, so allowing for that with inverse fourth-power dose-resolution scaling (Sayre *et al.*, 1977; Schneider, 1998) [$(30/20)^4 \simeq 5$] we see that the lower resolution requires five times lower 'Rose' dose than quoted for a 20 nm feature. The conclusion of all this is that 10^8 Gy is about ten times more dose than needed for Rose-criterion image quality at the planned ALBA resolution of 30 nm. We can therefore reasonably take the dose of 10^8 Gy to be characteristic of a 'good' image under ALBA operating conditions and we can use the latter to estimate exposure times. In addition, we can use the fact that the dose is proportional to the number of absorbed X-rays in a voxel (proportional to the signal-to-noise ratio squared) to deduce that the benefit of ten times more dose is $10^{1/2} \simeq 3.2$ times higher signal to noise than the Rose criterion. That is, our standard good image will have a signal-to-noise ratio of $3.2 \times 5 \simeq 16$.

The above discussion raises the question of why the ALBA team has adopted a routine resolution goal of 30 nm. We may cite the following considerations.

(i) It is reliably within technical reach without unreasonable delay.

(ii) The zone plates involved will have reasonable efficiency, focal length and depth of focus from the standpoint of tomography.

(iii) It will not be necessary to work near the limit of the modulation transfer function of the zone plate.

(iv) Although the resolution is substantially inferior to typical electron-microscope resolution values, the combined resolution and penetration power of the proposed ALBA microscope has been judged by the user community, many of whom are electron microscopists, to promise an immediate impact on some of their problems.

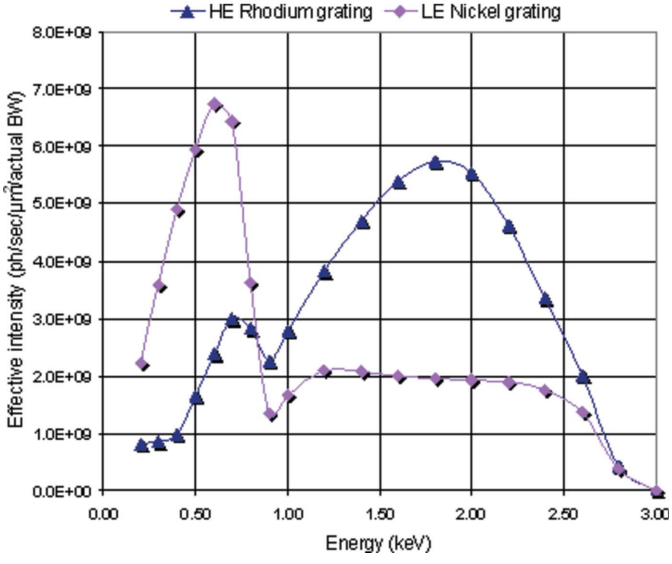

Figure 4
Effective X-ray intensity illuminating the sample allowing for optical elements efficiencies and capillary wobbling but not losses at slits. A capillary reflectivity of 0.7 and a capillary collecting factor of 0.44 have been used for the calculation.

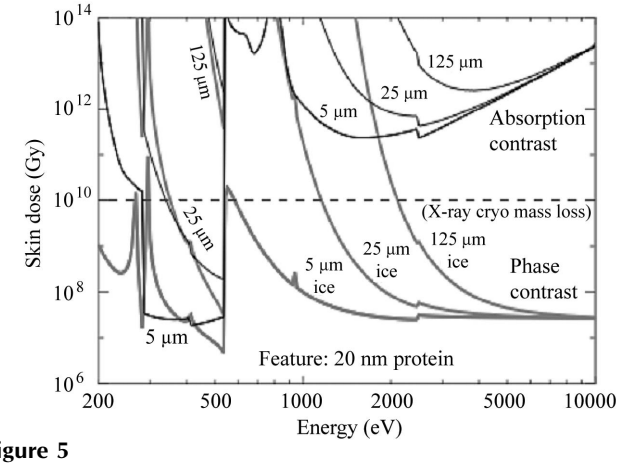

Figure 5
Dose required for imaging a 20 nm-cube protein voxel in various thicknesses of ice calculated for a signal-to-noise ratio of 5 [from Howells *et al.* (2007) following Kirz *et al.* (1995) calculations].

Now, returning to the notion of a standard 'good' image corresponding to an applied dose of 10^8 Gy, we begin by applying the 'dose fractionation theorem'. This was originally introduced by Hegerl & Hoppe (1976) and extended by McEwen *et al.* (1995). We can argue that the dose required for three-dimensional tomography of an object is the same as for the two-dimensional image of the same object provided that the resolution and statistical accuracy are the same in both cases. Of course, the 10^8 Gy will then be 'fractionated' over at least a hundred projections so each view will be of poor optical quality which is what one expects in minimum-dose imaging.

Using a dose of 10^8 Gy as a criterion, we can estimate the imaging time of the MISTRAL beamline and microscope (see Fig. 6). One sees that, even in the worse case, 30 s at 2600 eV, the exposure time will be considerably less than the other tasks involved in making a full tilt series (*i.e.* installing the sample, motor motions, detector readouts, flat field recordings *etc.*).

In the above discussion we have assumed that alignment of projections is carried out only off-line prior to volume reconstruction, as the axial run-out of the rotation stage is expected to be small enough (*i.e.* <0.5 µm) to allow this.

Now that we have established that 10^8 Gy is enough to produce a good image at our target resolution of 30 nm, we have to ask whether 30 nm features of a frozen-hydrated biological sample can withstand a dose of that level. This question has been addressed by Howells *et al.* (2008) who made a compilation of results from both the X-ray and electron literature, mostly 'spot-fading' experiments, which showed that 10^8 Gy is the critical dose for loss of detail at approximately the 1 nm level. This is far below the 30 nm level sought in the ALBA microscopy program so we conclude that our proposed system will produce rapid imaging of frozen hydrated samples which will be able to tolerate the required dose.

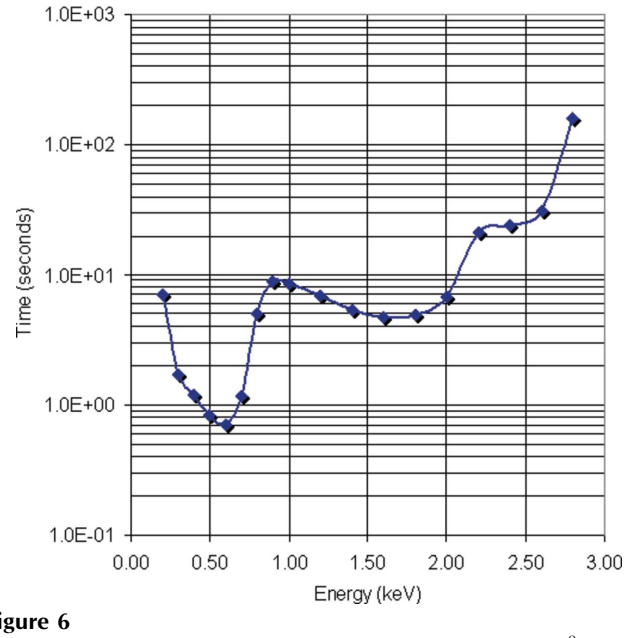

Figure 6
Exposure time for a 'good' image taken to be an exposure of 10^8 Gy. The theoretical efficiency of the objective zone plate has been calculated depending on the working energy for Ni (*e.g.* 833 zones, 100 µm diameter, 210 nm thickness) and Pt (*e.g.* 833 zones, 100 µm diameter, 450 nm thickness) zone plates, while the detector efficiency is assumed to be 100%. The condenser collecting factor was taken to be 0.44 and its reflectivity 70%.

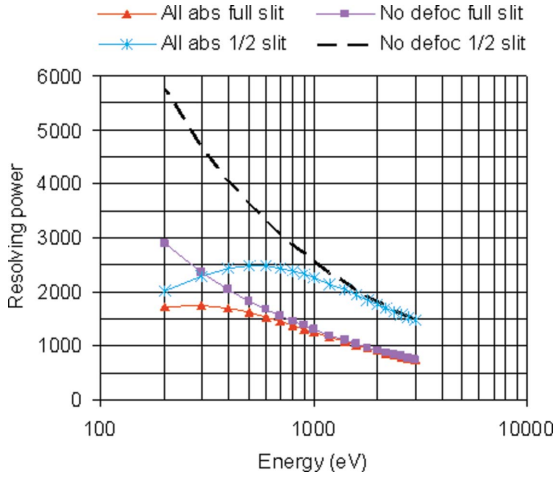

Figure 7
Monochromator resolving power in several cases. The variables are full slit width (set to collect most of the beam, *i.e.* 30 µm), half slit width (*i.e.* 15 µm), all aberrations as delivered by the VLS grating without further correction and, lastly, defocus corrected exactly (by a slit movement of less than 2 mm).

For spectromicroscopy, one of the other applications in addition to tomography that will be available at the MISTRAL beamline, a somewhat higher energy resolution is required. For example, 0.1 eV is necessary to resolve NEXAFS spectral features at the C 1*s* edge, which is one of the interesting edges in the water window range. The resolving power of the MISTRAL monochromator is presented in Fig. 7. The triangle-markers curve shows standard operation for imaging with 30 µm entrance slits, 15 µm exit slits and no focus correction. The square-markers curve shows the improvement obtained by having the exit slit position adjusted for exact focus by a few millimeters (*i.e.* 1.6 mm is the maximum correction at lower energy). When performing spectroscopic imaging, smaller slit openings will be used. Indeed, they will be closed at half the standard openings for imaging (*i.e.* 15 µm and 8 µm, respectively). This is shown with the star-markers curve, which is the same as the triangle-markers standard imaging curve without focus correction. Finally, the dashed curve represents the resolving power with both 'small' slits openings and focus correction. This last dashed curve shows the highest resolving power that will be achieved at the beamline.

6. Conclusions and outlook

We believe that the VLS PGM design is well matched to a microscopy beamline at a BM port mainly dedicated to cryotomographic imaging of biological samples. This variant of the VLS concept has large angular acceptance, is flexible (c_{ff}

can be freely varied) and is essentially aberration-free in the energy range of interest to us.

We expect that the ALBA X-ray microscope and beamline will be useful for biological imaging providing complementary capabilities to visible-light and electron microscopes. In particular, it will have an advantage in resolution over visible light imaging and in sample size over electron microscopy. We calculate that the integrated dose applied to the sample will be well below the damage limit for 30 nm features when the signal-to-noise ratio is about three times the Rose criterion (*i.e.* $10^{1/2} \times 5 \simeq 16$).

APPENDIX *A*
VLS monochromator design

A1. Introduction

VLS designs for synchrotron beamlines were developed in the early 1980s, as reviewed, for example, by Howells & Staub (1996). The principle pioneers were Harada (Harada & Kita, 1980; Harada *et al.*, 1984), mainly from a grating-manufacture viewpoint, and Hettrick (Hettrick, 1984, 1985), mainly from a spectrometer-design viewpoint. The paper by Howells & Staub (1996) has been useful in developing the VLS monochromator design for the ALBA beamline because it shows analytically how the VLS coefficients can be chosen to correct aberrations in a way that is independent of the wavelength and dependent only on the validity of the small-angle approximation. This leads to reasonable correction over a wide wavelength range, tending towards exact correction at short wavelength. However, it does not give the optimum design over shorter wavelength ranges.

A2. Magnification of a small source by an equal-line-spacing (ELS) grating

The focusing condition for any plane grating with equal groove spacing is given by writing down the standard focusing equation for a spherical grating (which normally yields the Rowland-circle condition) and letting the radius tend to infinity. The result is

$$r' = -r\frac{\cos^2\beta}{\cos^2\alpha} = -rc_{ff}^2 \qquad \text{where } c_{ff} = \frac{\cos\beta}{\cos\alpha}, \tag{1}$$

where r and r' are defined in Fig. 3 and α and β are given in §3. The minus sign indicates that the image of a real object will be virtual and *vice versa.* In addition, we can derive from the grating equation an expression for the magnification which is true for both equal- and variable-line-spacing gratings, as follows,

$$M = -\frac{r'}{r}\frac{\cos\alpha}{\cos\beta}. \tag{2}$$

Now substituting from (1) for $-r'/r$ we find for the equal-spacing case

$$M_{\rm ELS} = c_{ff}. \tag{3}$$

Thus in the usual case of $c_{ff} > 1$ (inside order, which we define as positive) we have an image magnified by a factor c_{ff} and a beam angular spread diminished by $1/c_{ff}$.

A3. Magnification of a small source by a VLS grating

A general conclusion of most of the literature has been that good properties of the VLS system can be obtained when the nominal focus is at or near $r' = -r$, the 'plane mirror' image point. Again, either the source or its image must be virtual. When $r' = -r$, the image is also stigmatic which is a distinct advantage. When we substitute this condition into the expression for the magnification (2), we find

$$M_{\rm VLS} = 1/c_{ff}, \tag{4}$$

indicating that, conversely to the ELS case, we now have an image size diminished by $1/c_{ff}$ and a beam angular spread magnified by c_{ff}.

A4. Specification of the grating groove positions

Following Padmore *et al.* (1998), McKinney (1992) and McKinney & Palmer (1989), we will initially define the groove positions according to

$$d(w) = d_0\left(1 + \nu_1 w + \nu_2 w^2 + \ldots\right). \tag{5}$$

An equivalent definition of the grating, up to any given accuracy, can also be obtained using the following series for the groove frequency $s(w)$ provided that N is large enough,

$$s(w) = s_0 + s_1 w + s_2 w^2 + \ldots + s_N w^N. \tag{6}$$

By considering $w = 0$, we can see that $s_0 = 1/d_0$, so $s(w)$ is given by s_0 times the reciprocal of the power series $(1 + \nu_1 w + \nu_2 w^2 + \ldots)$. For given ν_i, s_i can be calculated up to any N (Gradshsteyn & Ryzhik, 1980) and checked by comparison of the resulting $s(w)$ with the exactly known value of $1/d(w)$.

A5. Expressing the optical path function VLS coefficients directly in terms of the groove frequency

The quantity required for making calculations with the optical path function is n, the groove number, which becomes a non-linear function of w in a VLS grating. n is defined by

$$\frac{1}{d(w)} = s(w) = \frac{\partial n}{\partial w}, \tag{7}$$

and is taken to be zero at the grating pole ($w = 0$). $s(w)$ is defined by equation (6) from which we see that

$$\left.\frac{\partial^i s}{\partial w^i}\right|_{w=0} = i!\, s_i \tag{8}$$

and therefore, using (7), that

$$\left.\frac{\partial^i n}{\partial w^i}\right|_{w=0} = (i-1)!\, s_{i-1}. \tag{9}$$

The Taylor series for n, whose terms will determine the contribution of the VLS ruling to individual aberrations, can now be written as

$$n(w) = n(0) + \sum_{i=1}^{\infty} \frac{1}{i!} \frac{\partial^i n}{\partial w^i}\bigg|_0 w^i. \quad (10)$$

Substituting the above value for the derivative and using $n(0) = 0$, we obtain

$$n(w) \equiv \sum_{i=1}^{\infty} n_{i00} w^i = \sum_{i=1}^{\infty} \frac{s_{i-1}}{i} w^i, \quad (11)$$

so that

$$n_{i00} = \frac{s_{i-1}}{i}. \quad (12)$$

A similar calculation for n_{i00} in terms of the υ_i values has been carried out by McKinney (1992) and is available to the sixth order by Howells (2001). We show these for completeness,

$$\begin{aligned}
&n_{100} = 1/d_0, \qquad n_{200} = (-\nu_1)/2d_0, \qquad n_{300} = \left(\nu_1^2 - \nu_2\right)/3d_0,\\
&n_{400} = \left(-\nu_1^3 + 2\nu_1\nu_2 - \nu_3\right)/4d_0,\\
&n_{500} = \left(\nu_1^4 - 3\nu_1^2\nu_2 + \nu_2^2 + 2\nu_1\nu_3 - \nu_4\right)/5d_0,\\
&n_{600} = \big(-\nu_1^5 + 4\nu_1^3\nu_2 - 3\nu_1^2\nu_3 + 2\nu_2\nu_3 - 3\nu_1\nu_2^2\\
&\qquad + 2\nu_1\nu_4 - \nu_5\big)/6d_0. \quad (13)
\end{aligned}$$

The apparent simplicity of using the groove-frequency representation [equation (12)] is very striking.

A6. Choosing the VLS groove-frequency coefficients to correct their corresponding aberrations

Obviously we would like to choose each of the VLS coefficients n_{i00} so as to correct the corresponding in-plane aberration, in other words to solve the equation

$$F_{i00} + n_{i00} m\lambda = 0 \quad (14)$$

for n_{i00}. Howells & Staub (1996) have shown that, within the small-angle assumption, wavelength-independent solutions ['small-angle-optimum' (SAO) values of n_{i00}] can be found when $r' = -r$,

$$n_{i00}^{(\mathrm{SAO})} = \frac{1}{d_0 r^{i-1}}, \qquad i = 1, 2, 3, 4. \quad (15)$$

One can show that (15) is actually true for all values of i, again within the small-angle approximation, by considering the dominant term of each F_{i00} coefficient for higher i values. For a plane grating, such terms are always of the form

$$F_{i00} = \frac{\cos^2\alpha \sin^{i-2}\alpha}{2r^{i-1}} + \frac{\cos^2\beta \sin^{i-2}\beta}{2r'^{i-1}}. \quad (16)$$

Using this and $r' = -r$ in equation (14), plus the small-angle assumption, does indeed lead to equation (15) for all i values.

By means of equation (12), we can now obtain a similar rule for the optimum s_i coefficients,

$$s_i^{(\mathrm{SAO})} = \frac{i+1}{d_0 r^i}. \quad (17)$$

Moreover, now that we have the values of $n_{i00}^{(\mathrm{SAO})}$, we can substitute them into equation (13) starting at low order and progressively obtain $\nu_i^{(\mathrm{SAO})}$. The results are simple and surprising,

$$\nu_1^{(\mathrm{SAO})} = \frac{-2}{r}, \quad \nu_2^{(\mathrm{SAO})} = \frac{1}{r^2}, \quad \nu_i^{(\mathrm{SAO})} = 0 \text{ otherwise.} \quad (18)$$

Thus the groove-spacing representation also has some simple properties. Moreover, to make a VLS grating by programming a ruling engine, it is the groove spacing or its integral, the groove position, that is required. Perhaps holographic schemes can be thought of naturally in frequency terms.

The values of $n_{i00}^{(\mathrm{SAO})}$, $\nu_i^{(\mathrm{SAO})}$ and $s_i^{(\mathrm{SAO})}$ derived above are estimates of the optimum values for aberration cancelling by VLS over a large energy range. There are ways to obtain better performance over limited energy ranges which we do not discuss here. The amount of uncorrected aberration under this scheme approaches zero as zero order is approached. The correction degrades gradually as one moves away from zero order. For example, the defocus error in the MISTRAL system that we are reporting here grows from zero at zero order to 1.6 mm at 4.5 nm wavelength (the beamline maximum). One's perception of what 'gradually' means depends on the resolution that is being sought and the energy range involved. The predicted energy resolution, energy range and other measures of the performance of the ALBA X-ray microscope beamline are given in the main text.

References

Andrews, J. C., Brennan, S., Patty, C., Luening, K., Pianetta, P., Almeida, E., van der Meulen, M. C. H., Feser, M., Gelb, J., Rudati, J., Tkachuk, A. & Yun, W. B. (2008). *Synchrotron Rad. News*, **21**, 17–26.

Born, M. & Wolf, E. (1980). *Principles of Optics.* Oxford: Pergamon Press.

Follath, R. & Senf, F. (1997). *Nucl. Instrum. Methods Phys. Res. A*, **390**, 388–394.

Gradshsteyn, I. S. & Ryzhik, I. M. (1980). *Tables of Integrals, Series and Products.* Item 0.314. New York: Academic Press.

Harada, T., Itou, M. & Kita, T. (1984). *Proc. SPIE*, **503**, 114–118.

Harada, T. & Kita, T. (1980). *Appl. Opt.* **19**, 3987–3993.

Hegerl, R. & Hoppe, W. (1976). *Z. Naturforsch. Teil A*, **31**, 1717.

Hettrick, M. C. (1984). *Appl. Opt.* **23**, 3221–3235.

Hettrick, M. C. (1985). *Proc. SPIE*, **560**, 96.

Howells, M., Jacobsen, C. & Warwick, T. (2007). *Principles and Applications of Zone Plate X-ray Microscopes*, ch. 13, *Science of Microscopy*. New York: Springer.

Howells, M. R. (2001). *X-ray Data Booklet (PUB 490)*, edited by A. Thompson and D. Vaughan. Center for X-ray Optics, Lawrence Berkeley Laboratory, CA, USA. (http://www-cxro.lbl.gov/.)

Howells, M. R., Beetz, T., Chapman, H. N., Cui, C., Holton, J. M., Jacobsen, C., Kirtz, J., Lima, E., Marchesini, S., Miao, H., Sayre, D. E., Shapiro, D. A., Spencer, J. C. H. & Starodub, D. (2009). *J. Electron Spectrosc. Relat. Phenom.* **170**, 4–12.

Howells, M. R. & Staub, U. (1996). PSI report 96–20. ISSN 1019-0643.

Kirz, J., Jacobsen, C. & Howells, M. R. (1995). *Q. Rev. Biophys.* **28**, 33–130.

Larabell, C. A. & Le Gros, M. A. (2004). *Mol. Biol. Cell*, **15**, 957–962.

McEwen, B. F., Downing, K. H. & Glaeser, R. M. (1995). *Ultramicroscopy*, **60**, 357–373.

McKinney, W. R. (1992). *Rev. Sci. Instrum.* **63**, 1410–1414.

McKinney, W. R. & Palmer, C. (1989). *Proc. SPIE*, **1055**, 332–335.

Niemann, B., Rudolph, D. & Schmahl, G. (1974). *Opt. Commun.* **12**, 160–163.

Padmore, H. A., Howells, M. R. & McKinney, W. R. (1998). *Techniques of Vacuum Ultraviolet Physics*, edited by. J. A. R. Samson and D. Ederer. Orlando: Academic Press.
Petersen, H. (1982). *Opt. Commun.* **40**, 402–406.
Rose, A. (1948). *Advances in Electronics*, Vol. 1, edited by L. Martin, p. 131. New York: Academic Press.
Sayre, D., Kirz, J., Feder, R., Kim, D. M. & Spiller, E. (1977). *Ultramicroscopy*, **2**, 337–349.
Schäfers, F. & Krumrey, M. (1996). Technical Report TB 201, pp. 1–17. BESSY, Berlin, Germany.
Schneider, G. (1998). *Ultramicroscopy*, **75**, 85–104.
Schneider, G., Anderson, E., Vogt, S., Knöchel, C., Weiss, D., Le Gros, M. & Larabell, C. (2002). *Surf. Rev. Lett.* **9**, 177–183.
Schneider, G., Guttmann, P., Heim, S., Rehbein, S., Eichert, D. & Niemann, B. (2006). *AIP Conf. Proc.* **879**, 1291–1294.
Tang, M.-T., Yin, G.-C., Song, Y.-F., Chen, J.-H., Tsang, K.-L., Liang, K. S., Chen, F.-R., Duewer, F. & Yun, W. (2006). *Proceedings of the 8th International Conference on X-ray Microscopy (XRM2005)*, Series 7, Himeji, Japan, pp. 15–17.
Thieme, J. (1988). *X-ray Microscopy II, Springer Series in Optical Sciences*, edited by D. Sayre, M. R. Howells, J. Kirz and H. Rarback. Berlin: Springer-Verlag.
Yin, G.-C., Tang, M.-T., Song, Y.-F., Chen, F.-R., Liang, K.-S., Duewer, F., Yun, W., Ko, C.-H. & Shieh, H.-P. D. (2006). *Appl. Phys. Lett.* **88**, 241115.
Zhang, W., Ge, S., Wang, Y., Rafailovich, M. H., Dhez, O., Winesett, D. A., Ade, H., Shafi, K. V. P. M., Ulman, A., Popovitz-Biro, R., Tenne, R. & Sokolov, J. (2003). *Polymer*, **44**, 2109–2115.
Zheng, X., Duewer, F., Feser, M., Huang, C., Lyon, A., Tkachuk, A. & Yun, W. (2008). *Appl. Opt.* **47**, 2376–2381.